AIAA Propulsion and Energy Forum
19-22 August 2019, Indianapolis, IN
AIAA Propulsion and Energy 2019 Forum

10.2514/6.2019-3988

Erosion of meshed reflector in the plume of a Hall effect thruster, Part 2: Experiments

Matthew P. Byrne*, Mackenzie E. Meyer†, Iain D. Boyd‡,and Benjamin A. Jorns§
University of Michigan, Ann Arbor, MI, 48109, USA

An investigation into the erosion of a reflector mesh in the plume of a Hall effect thruster is presented. Representative samples of the meshed reflector material are exposed to different regions of the thruster plume, and the erosion due to ion bombardment is characterized. Part 1 of this study documents the development of a model to predict the erosion of the wires which comprise the mesh. In this report, Part 2, the predictions of that model are experimentally validated. First, detailed measurements of the plume are performed using a suite of plasma probes. Second, erosion predictions based on these measurements are directly compared to experimentally measured erosion profiles. The erosion model is shown to predict qualitatively the eroded shapes of the wires in all cases, exhibiting peaks along the direction of normal incidence. Quantitatively, when based on the measured plume properties, the model predictions agree with the measured erosion of the wires to within 0.1 wire radii near normal incidence but overpredict the erosion by up to 0.4 wire radii near the wire edges where the ions impact at more oblique angles. These results are discussed in the context of uncertainty in known sputtering models and the highly nonlinear dependence of sputtering on incident angle.

Nomenclature

EP	Electric Propulsion
E	Incident Ion Energy
E_o	Sputtering Threshold Energy
$Y(E,\theta)$	Sputtering Yield
θ_{opt}	Optimal Sputtering Angle
Δx	Erosion Depth
Δt	Exposure Time
j_i	Ion Current Density
q	Ion Charge
m	Mass of Target Element
ρ	Target Density
$LVTF$	Large Vacuum Test Facility
$H6US$	H6 Hall Thruster
JPL	Jet Propulsion Laboratory
FP	Faraday Probe
GRC	Glenn Research Center
RPA	Retarding Potential Analyzer
$MPIC$	MONACO-PIC

I. Introduction

Electric propulsion (EP) is a popular choice for both commercial and governmental space missions [1]. The ability of these systems to accelerate propellant to high exhaust velocity translates to higher propellant efficiency and mass savings when compared to alternative forms of propulsion. EP systems thus can facilitate missions at a substantially

*Ph.D. Candidate, Applied Physics, AIAA Student Member.
†Ph.D. Pre-Candidate, Applied Physics, AIAA Student Member.
‡James E. Knott Professor, Department of Aerospace Engineering, AIAA Fellow
§Assistant Professor, Department of Aerospace Engineering, AIAA Senior Member.

reduced cost. On the other hand, the capability to produce high velocity propellant also can pose a risk to the overall spacecraft if any of the vehicle's surfaces are in the path of the thruster's exhaust. [2]. Indeed, elements exposed to even a low ion flux can be damaged over the long periods of thruster operation typical for EP-powered missions. This source of erosion is particularly problematic for large-scale communication dishes as these components often are deployed beyond the spacecraft and will intercept a portion of the EP system's exhaust plume.

Given the potential risk posed by the thruster plume to payload surfaces, there have been a series of studies, both experimental [3, 4] and computational [5–7] to predict the sputtering of various common spacecraft materials caused by EP plumes. From investigations like these, others have developed a variety of empirical models to predict sputtering rates [8–15]. While these models have yielded insight and guidance into the erosion of spacecraft surfaces subject to thruster plumes, their applicability to communication dish reflector meshes is limited. Indeed, there are two issues precluding these use of these models for these complicated geometries. The first is that the wires that comprise the mesh have a curved surface. As a result, the planar sputtering models from the literature are not directly applicable as the ion incidence angle varies over the surface of the wire. The second issue is that most of these models assume that the ion source is nearly mono-energetic, whereas the exhausts of many typical forms of EP systems (such as Hall thrusters) typically have extended ion energy distributions which vary in shape throughout the plume. The net implication is that to date there is yet to be an erosion model with sufficient geometric and plasma plume fidelity to evaluate the erosion of reflector surfaces. Given this limitation and the widespread use of these communications dishes on spacecraft buses with electric propulsion, there thus is a pressing need for an experimentally validated model to predict the erosion of these mesh wires. Part 1 of this study [17] documents the development of the erosion model for the cylindrical geometry of the mesh wire. This part, Part 2, presents the experimental verification of the model predictions when based on both experimentally measured and simulated plume properties.

This paper is organized in the following way. In the first section, we discuss the theory behind the erosion model for curved surfaces developed in Part 1 of this study [17]. We then describe the setup for two experiments we performed with test coupons placed in the plume of a Hall thrusters to validate the erosion model predictions. This is followed by a presentation of the results of these experiments and a comparison of these measurements to model predictions. Finally, we draw conclusions about the validity and limitations of the erosion model in light of the experimental findings.

II. Erosion Model Overview

This erosion model for reflector wires is presented in detail in Part 1 [17]. We briefly review here its key features. The typical geometry for a reflector consists of an interlaced network of mesh wires. These mesh wires are composed of a molybdenum core which has been clad in a gold. A notional cross section of a wire is shown on the left side of Fig.1. The wire dimensions have been normalized to its radius. As discussed in part 1, we model the erosion of this geometry first by discretizing the wire surface into a series of planar sections. This has the benefit of allowing us to estimate the erosion locally at each planar section with the standard sputtering equation:

$$\frac{\Delta x}{\Delta t} = Y(E,\theta)\frac{j_i}{q}\frac{m}{\rho}, \tag{1}$$

where Δx is the change in depth, Δt is the exposure time, j_i is the ion current density, q is the ion charge, m is the atomic mass of the target element, ρ is the density of the target, and $Y(E,\theta)$ is the sputtering yield (atom per incident atom) of the material. This expression shows how the rate of erosion depends both on the rate of flux of sputtering particles to the surface as well as the energy, E, and angle of incidence, θ. In the process described in Part 1, the erosion model begins by calculating the ion incidence angle of each planar element. It then uses a sputtering model selected from the literature to calculate the total sputtering yield based on the calculated angle and local ion energy. Next, the model calculates the erosion depth from the sputtering yield and local ion current density. The discretized planes are then moved along lines normal to the surface a distance equal to the calculated depth. Finally, the surface endpoints are averaged to generate a new set of planar elements. In this way, the wire surface can be steadily advanced in time, evolving into new shapes dictated by the sputtering yield and incident plasma properties.

As be seen from Eq. 1, the erosion calculation depends on having measurements or models for two key sets of parameters. The first set is comprised of the mechanical and structural properties of the material itself and is related to the sputtering yield. For most treatments of the sputtering process, it is typically quantified by an analytical equation, which takes in values of ion energy and incidence angle and outputs the sputter yield in terms of target atoms sputtered per incident ion. It is expressed as the product of two contributions,

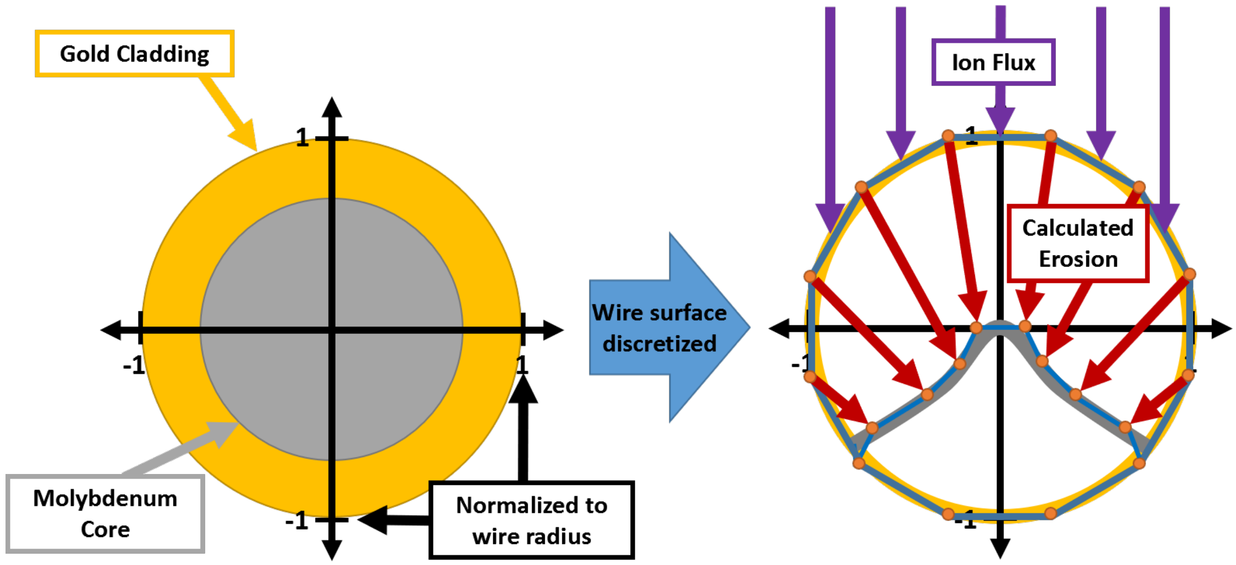

Fig. 1 Diagram showing a notional wire cross section (left), and a cartoon representation of the erosion model (right) documented in Part 1 [17].

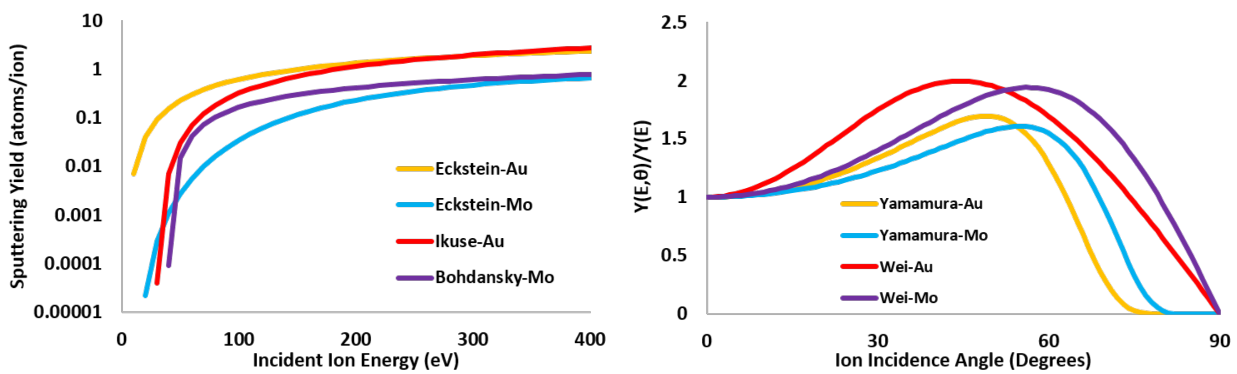

Fig. 2 Examples of the energy dependence(left) and incident angle dependence (right) of the sputtering yield induced by xenon atoms on Au and Mo for different sputtering models . The incident ion energy is 250 eV for the angular dependence plot.

$$Y(E,\theta) = Y(E) \cdot Y(\theta), \tag{2}$$

where $Y(E)$ can be interperted as the sputtering yield for normally incident ions as a function of energy and $Y(\theta)$ is the sputtering dependence on the angle of incident with respect to the surface normal. We show examples of models for both normal incidence and angular incident sputtering in Fig. 2. As the normal incidence graph shows, there is a cutoff energy where no sputtering, a plateau region where sputtering is largely independent of the incident energy, and a rapid increase in sputtering at some threshold value. We also depdict in this figure a typical results for the angular dependence of gold and molybdenum. These results illustrate a key feature: there is a peak in the sputtering yield at some off-normal ion incidence angle where the yield can be many times higher than normal incidence. We show here the five different models for both normal incidence and angular incidence sputtering that were used in the sputtering calculations performed in Part 1. This includes three normal incidence models from Ikuse [11], Bohdansky [13], and Eckstein [9], and two angular incidence models from Yamamura [12] and Wei [10].

The second set of data needed to evaluate the erosion from the model in Part 1 (per Eq.1) consists of the local plasma properties at the mesh surface including ion current density, incident energy, and local angle with respect to the discretized surface. We consider in this work (and Part 1) two sources for this plasma data. The first and higher fidelity is comprised of experimental data measured directly in the plume of a thruster where the wire is located. This source of data has the most utility for evaluating the ability of the model to predict erosion as it provides exact assessments of most of the parameters in Eq. 1. The second source of data we employ is based on plume properties generated from a high-fidelity plume model. The validation against this data demonstrates the ability of the wire erosion model to work in conjunction with the types of plume models typically employed by spacecraft integrators to predict the thruster environment on orbit where experimental measurements are not available. To this end, the model used in Part 1 consists of the 2D axisymmetric simulation MONACO-PIC (MPIC) [18]. This model has been applied extensively in spacecraft plume interactions and is thus a well-suited tool for providing simulation plume data. Though, as discussed in the following, it was necessary to calibrate he MPIC plume model for a given thruster geometry against experimental measurements. This was done in Part 1 by adjuting the inlet conditions to match the plume measurements for the test article we describe in the following section.

III. Experimental Setup

There are two steps needed to validate the erosion model predictions from Part I. The first is to compare the results from our erosion model to experimental results when the plume parameters the wire is exposed to are well known. The second step is to calibrate the predictions so that when a plume model is also used, the predictions agree with the experimental results. We describe in this section the setup for two experiments to accomplish these ends. In the first experiment, a probe suite was swept through the plume of an operating thruster and the ion current density, ion energy distributions, and ion charge state populations were measured. In the second experiment small samples of the meshed reflector material were exposed to different regions of the plume and the resulting erosion was characterized.

A. Thruster and Facility

Both experiments were conducted in the Large Vacuum Test Facility (LVTF) at the University of Michigan's Plasmadynamics and Electric Propulsion Laboratory. LVTF is a 9 m long and 6 m diameter vacuum chamber. At the time of these experiments, eight TM-1200 cryogenic pumps and five copper cryosails chilled by cryomech compressors provided the pumping capacity for the facility. The pressure in the chamber was measured at the exit plane of the thruster 1 m from the thruster centerline by an MKS 370 Stabil-Ion pressure gauge, in keeping with industry standard [19]. The thruster was fed with 99.995% Xenon through two Alicat MC mass flow controllers. The base pressure was 0.5 μTorr on average, and increased to 10 μTorr when the truster was firing.

The thruster used in this study was the non-magnetically shielded H6 Hall thruster (H6US), a 6-kW Hall thruster that was jointly developed by the University of Michigan, Air Force Research Lab, and the NASA Jet Propulsion Laboratory. We chose this thruster due to its availability and the large amount of publications documenting its operation [20–26]. For both of our experiments the H6US was operated at a 300 V, 3 kW operating condition. It utilized a 20 A LaB_6 hollow cathode at a 7% flow fraction. The thruster body was grounded for the duration of the tests.

B. Plume Characterization

In order to characterize the plasma properties of the H6US in the plume regions of interest, a suite of plasma probes was affixed to a rotation stage by a 1 m arm. The probe suite consisted of three different plasma probes, a Faraday probe (FP) for measuring ion current, a retarding potential analyzer (RPA) for measuring ion energy distributions, and an E×B probe (also known as a Wein filter Spectrometer) for measuring the relative populations of ion charge states. Figure 3 shows a diagram of the experimental setup and pictures of the probe suite and rotation arm.

The Faraday probe used in this experiment was of NASA Glenn Research Center (GRC) design [27]. The collector and guard ring of this probe were made of Molybdenum and mounted to a macor back plate. The collector face was 1.74 cm in diameter and the guard ring had an outer diameter of 2.38 cm with a 5mm separation between them. During the experiment, both the collector and guard ring of the probe were biased to -60 V below ground so as to be in the ion saturation region. The probe was swept through the plume and measurements of the average ion current density were taken every 5 degrees from 0 to 90 degrees.

The RPA used in this experiment was of Air Force Research Lab design [27]. This probe had four different grids and a collector plate. The first grid was left floating, the second grid was biased to -30V to repel electrons, the third grid was swept from 0 to 400V to filter out ions of different energies, and the fourth grid was also biased to -30V to suppress secondary electron emission caused by high energy ions striking the collector. The probe aperture was 6.45cm^2. Like the FP the RPA was swept through the plume and ion energy distributions were measured every 10 degrees from 0 to 90 degrees.

The final probe in the suite was an E×B probe constructed at the University of Michigan from a NASA GRC design. The probe uses a magnetic field provided by permanent magnets and a perpendicularly oriented electric field provided by two bias plates to filter the ions in the plume based on charge state. The bias field was swept from 0 to 60V, and the collector was held at -5V to suppress secondary electron emission. Like the other probes the E×B was swept through the plume; however, damage to the experimental setup prevented more than one measurement from being taken successfully.

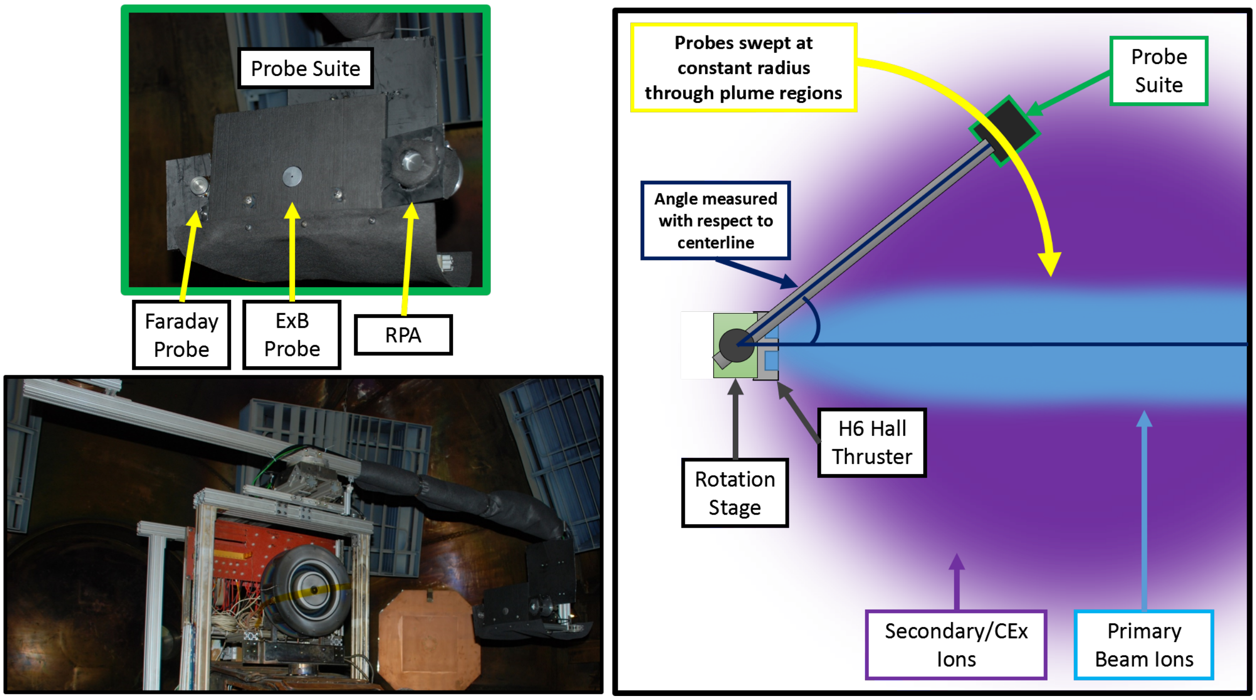

Fig. 3 Plume Characterization Experiment, A suite of plasma probes was used to measure the plume of the H6 operating at 300V-10A. The probe suite - consisting of a Faraday probe, an E×B probe, and a RPA - was swept through the plume from 0 to 90 degrees with respect to thruster centerline at a radius of 1 meter.

C. Wear Testing

In order to characterize the effects of the thruster plume on the reflector mesh, eight test coupons were exposed to different regions of the thruster plume for a duration of ten hours. Samples of the reflector mesh were epoxied into four inch square aluminum frames, using a high temperature Loctite EA9394 Aerospace epoxy. The samples were suspended from four aluminum test stands and spaced at eight different angles with respect to thruster centerline: 10°, 18°, 25°, 33°, 48°, 63°, 80°, and 90°. These angles were chosen to measure the effect of a wide variety of ion energies and current densities on the samples. All of the samples were placed at a one meter radius from the thruster on a single plane in line with the center of the thruster and then turned to face the center of the arc. This can be seen in Fig. 4. The black material seen in the photos is flexible graphite foil used to prevent the sputtering of the aluminum test stands and frames.

D. Optical Profilometry

The wire geometries were measured using a Olympus LEXT Laser Confocal Microscope. The microscope generates high resolution three-dimensional images by stitching together multiple images at different focal planes. It is capable of a vertical resolution of 10 nm, and a lateral resolution of 120 nm. Images and profile measurements of the samples were acquired at 100× magnification. At this magnification, the height measurements had an error of 0.2%.

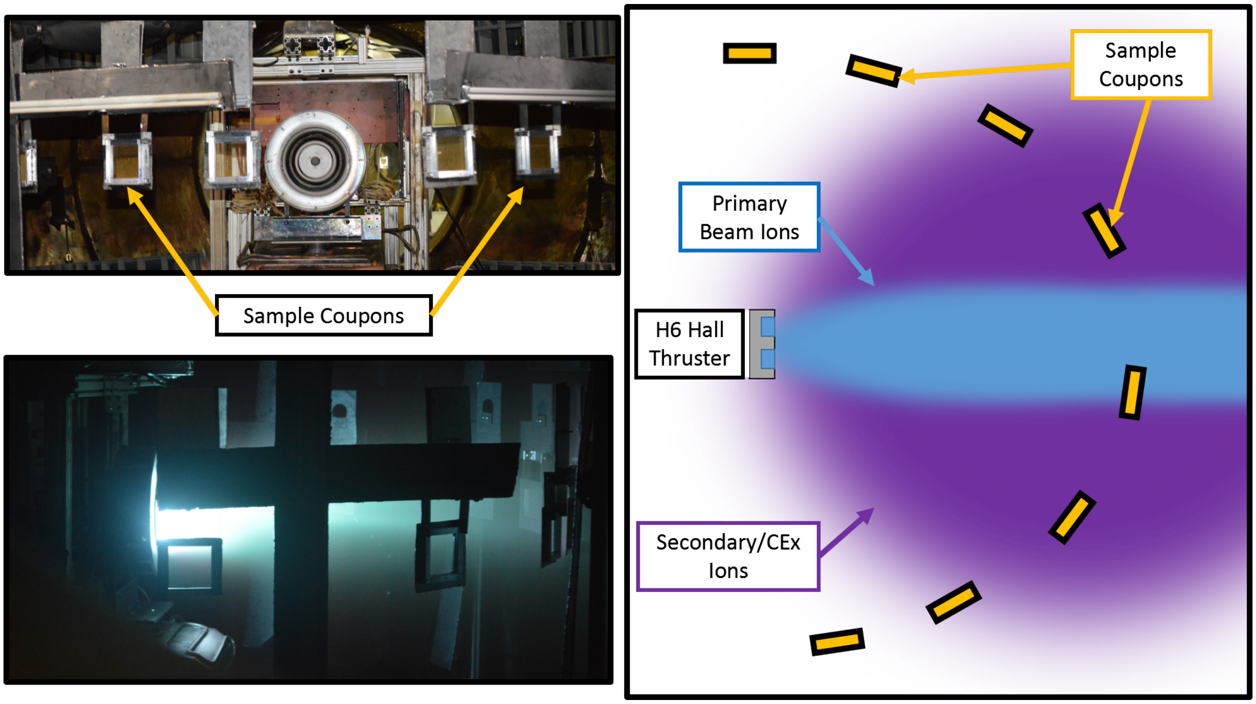

Fig. 4 Wear test setup where eight coupons of the meshed material were exposed to the plume of the H6 operating at 300V-10A for 10 hours. The samples were spaced equidistant from each other at a radius of 1 meter from the thruster.

IV. Results

In this section, we present the results from our two experimental campaigns and quantify the effects of the thruster plume on the test articles. From the first experiment, we discuss features of the FP, RPA, and E×B probe measurements. From the second experiment, we examine the pictures and profilometry measurements of test coupons before and after exposure to the thruster plume.

A. Plume Characterization

In the first experiment, we used a probe suite to obtain ion current density, ion energy distribution, and the relative populations of ion charge states across a 90 degree arc of the plume at a one meter radius. Fig. 5a shows the ion current density with respect to the probe arm angle measured from centerline. 0° is directly downstream of the thruster. This trace is typical for this thruster operating at these pressures with a well-defined peak that tapers off exponentially. This plot was generated by measuring the current density from 0 to 90°; the values were then mirrored to show the full distribution.

Fig.5b shows a plot of five ion energy distributions measured at different angles with respect to the thruster centerline. This, again, is a typical result. As the angle increases the distributions show that the plume shifts from primarily thermal and charge exchange ions to mostly beam ions. This is evidenced by the decreasing number of lower energy ions and the growth of the peak near the discharge voltage. The distributions were calculated by taking the derivative of the collected current with respect to the bias voltage; the plots were not corrected for plasma potential, which would cause at most a 15 V difference [24].

The final plot, Fig. 5c, shows the relative populations of ion charge states measured by the E×B probe. It demonstrates that while the plume is primarily composed of singly charged ions, about 85%, there is a non-insignificant population of multiply charged ions. These ions can contribute significantly to sputtering as they gain more energy from the discharge potential.

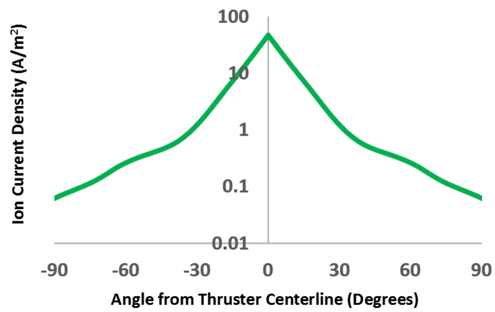

(a) Plot of the ion current density as a function of angle from thruster centerline.

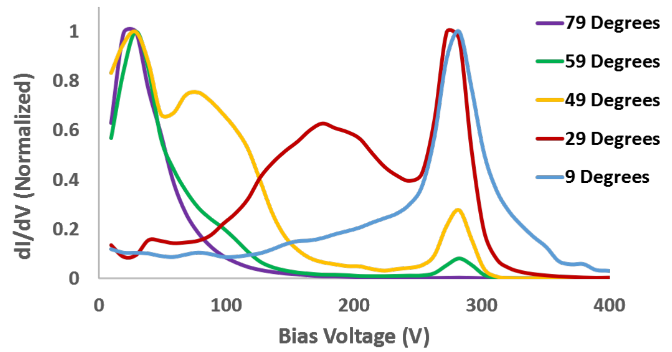

(b) Plot of a selection of ion energy distributions at different angles from thruster centerline

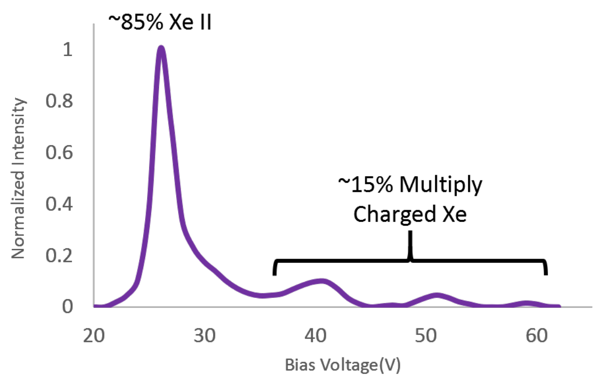

(c) Plot of the relative population of ion charge states at 30 degrees from thruster centerline.

Fig. 5 Results of the plume characterization experiment. All three measurements were taken at 1 m radius while the thruster was operating at 300 V 10 A condition.

B. Comparison between plume measurements and M-PIC simulations

As discussed above, although we had direct experimental measurements of the plume properties in the thruster exhaust to inform the erosion model, there is value in also demonstrating the ability of the erosion model to make predictions by using input from plume simulations. The MPIC simulation we used in part 1 for this purpose was in part calibrated on the plume data shown in Fig. 5. Fig. 6 illustrates a direct comparison of the calibrated model's outputs to the experimental data. The calibrations were performed by systematically adjusting the inlet parameters of the neutral atoms to better match the experimental results. This gave us good qualitative agreement between experiment and model, but there are some important quantitative differences. As can be seen, the ion current density curve had relatively good agreement with the experimental results at 35 degrees but diverged from these results at both lower and higher angles. At 10 degrees from centerline the predicted density was nearly double the measured density. The predicted ion energy distributions matched the experimentally measured peak but had significant discrepancies at lower ion energies. These differences are attributed to insufficient model fidelity at the effective inlet, as it currently does not have much experimental support or accommodate magnetic field effects. Ultimately, for Part 1 efforts, this relative degree of agreement was sufficient to evaluate the ability to integrate MPIC with the erosion model. Though, these discrepancies may ultimately be sources for error in prediction erosion as discussed in Sec. V.

C. Wear Testing

The purpose of the second experiment was to obtain actual measurements of the mesh wire erosion in the plume of a Hall effect thruster. We placed eight mesh sample coupons in the plume at a variety of locations to compare different

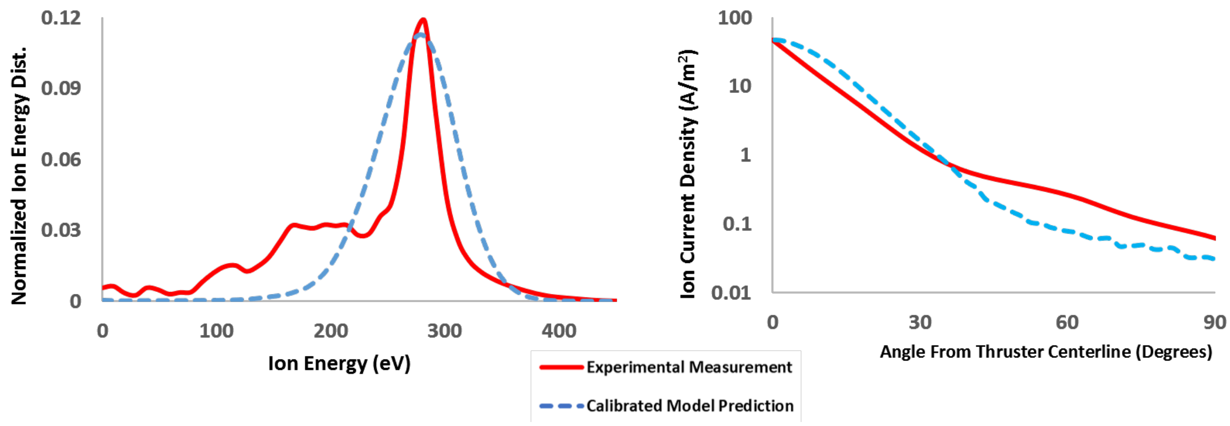

Fig. 6 Comparison between the experimentally measured plasma parameters, shown in red, and the predicted plasma parameters shown in blue. The IEDF on the left was measured at 18 degrees from thruster center line.

erosion points to the predictions. After the wear test, we quantified the erosion visually with a high-resolution photo as well as with the optical profilometer described in Sec. IIID. Examples of the results from both techniques are shown in Fig.7 for the oblique location at 48° in the plume. The gray surface in the image of the wire from this location reflects the fact that the original outer gold surface had been completely eroded. For the optical profilometery result, we measured each wire along a series of lines drawn from different locations in the longitudinal direction and compared it to the original surface of the uneroded wire (purple line). We consistently found that all of the line profiles agreed and exhibited qualitatively similar behavior with the photographic results. For the remainder of the results we present here, the experimental erosion measurements are based on averaging over five line profiles with uncertainty based on the standard deviation of these averages.

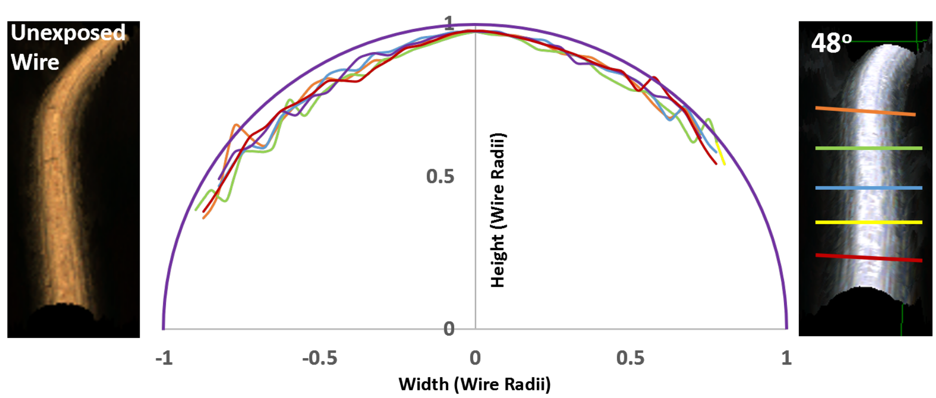

Fig. 7 Image of an unexposed wire and a wire from the sample at 48 degrees along with experimentally measured wire profiles from that sample at five different points along the wire surface.

Following this approach, we show the averaged optical profilomter results for each sample location from the plume in Fig.8. The purple ring represents the initial surface of an uneroded mesh wire, while the yellow line is an average of the measured profiles. We can see that the measurement of the unexposed sample agree very well with this border. The sample at 63° shows a small amount of erosion in only the gold layer of the mesh wires. At 48° we see that the outer surfaces of the wire has been sputtered away, exposing the molybdenum on the top surface of the wire. When the angle was reduced to 33° significant erosion of the wire can be seen, profoundly changing the profile into a pointed shape. At 18° the vast majority of the wire has been eroded away, leaving only a small sliver of material remaining. This abrupt change in the amount of erosion coincides with the transition from the wings of the plume into the main beam of the discharge.

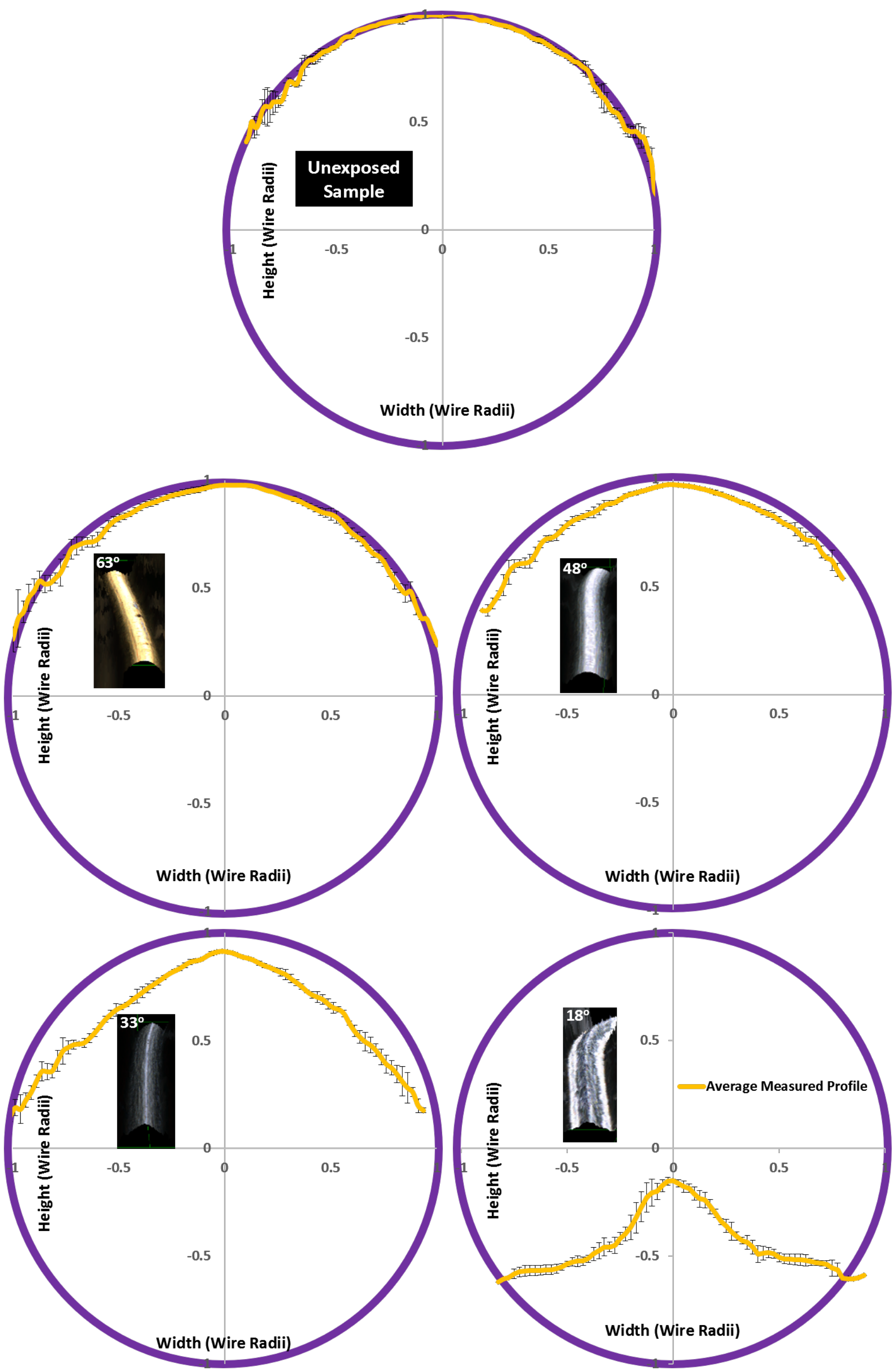

Fig. 8 Experimentally measured wire profiles for 5 different mesh samples exposed to different amounts of the plume of the H6US operating at 300 V-10 A for 10 hours. The purple ring represents the pre-erosion wire surface. The yellow line is an average of the experimentally measured profiles.

D. Erosion Model Comparison

Fig.9 shows a a direct comparison between the predictions of the erosion model and the measured wire profiles from the previous section. The averages of the experimentally measured profiles are shown as yellow lines where the variance results from irregularities in the wire surface at different measurement location. The blue dotted lines and solid red lines are the predicted wire geometries generated by the erosion model. For these results, the sputtering from the model was calculated from the Eckstein normal incidence model [9] and the Wei angular incidence model [10]. We show the Eckstein/Wei combination here because it was the best individual combination demonstrated in Part 1 The erosion of the red profiles was calculated using the experimentally measured plasma parameters presented in the previous section. Similarly, the blue dotted profiles were created using the plasma parameters from the calibrated plume model. The results of these comparisons show that the erosion model can predict the erosion of samples at larger angles very well. At 63 and 48 degrees, both the experimental data prediction and plume model predictions are in strong agreement with the measured profiles. The differences between them are lower than the measurement variance. However, the results also show that at angles closer to thruster centerline, both predictions began to diverge from the experimental profiles but still agree with the measurements to within 0.04 wire radii. At 33 degrees, the model predictions that use experimental data as inputs underestimate the erosion, while the model predictions that use simulated plasma data overestimated the erosion. Near normal incidence, both models are consistent with the measured profiles, agreeing within 0.1 wire radii. On the edges of the wire, however, they begin to disagree with each other by ~ 0.15 wire radii. Both predictions diverge by up to 0.4 wire radii from the measured profiles. At 18 degrees, the model predictions that used simulated data no longer gave physical results, and the model predictions that used experimental plume data disagree by up to 0.15 wire radii in the wings but they still agreed within the experimental variance at the top of the wire.

In summary, we find that the measured wire profiles are in good agreement with both erosion predictions for samples located at angles $\geq$48 degrees from centerline. At angles closer to centerline, near 33 degrees, the erosion predictions diverge slightly from the true profiles. The divergence is still within the measurement uncertainty near the center of the wire, but becomes worse near the edges. This pattern continues for the sample nearest to centerline, but the divergence is more pronounced. At this point, however, the predictions which use the simulated plume data no longer give realistic results. We discuss these observations in the following section, and explore their consequences for erosion predictions.

V. Discussion

In this section, we discuss our results and consider the strengths and limitations of the erosion model. We first consider the origin of the unusual peak-like structure of the eroded wires in Figs. 8 and 9. This result can be understood in the context of the high degree of angular dependence of the sputtering yield as shown in Fig. 2,where we see that sputtering is maximized at an off-normal ion incidence angle. Given this dependence, for a wire exposed to a beam, the edges of the wire (which have a higher local angle with respect to the incident beam) would erode more quickly than the center. This would cause the wire lose its circular cross section and become more pointed. The prediction is borne out by both the experimental profiles and the erosion model predictions. This validated the ability of the planar discretization approach used in the erosion model to predict eroded shapes.

With that said, although the model was able to capture this non-uniform erosion of the wire qualitatively in all cases, as can be seen from our results in Figs.8 and 9, it did not predict quantitatively the degree of erosion under all circumstances. From the comparisons we presented in the last section, we found that the model matches the experimental profiles well at locations where the ions struck at near normal incidence, but it displayed some discrepancies when the ion incidence became more oblique. In particular, it both overpredicts and underpredicts the erosion at the wire edges depending on the plume location. Whereas the divergence from measured profiles is small at 63 and 48 degrees, it becomes much more pronounced as the angle from thruster centerline is decreased.Samples placed closer to the primary beam are exposed to much greater ion flux. Any discrepancies in either the sputtering models or the erosion model from reality are accentuated by the increased erosion. One possible explanation is that our analysis ignores multiply charged ions which have the potential to significantly impact sputtering yields. From Fig.5c, we know that 15% of the ions in the plume at 30 degrees from centerline have been ionized more than once. Given the exponential nature of sputtering yields, accounting for the multiply charged ions at more points in the plume could reduce this divergence between model and result .

When a plume simulation was used in place of the experimentally obtained plasma parameters, the model predictions overestimated the erosion in samples at lower angles from centerline. This can be explained by noting that at angles above 30 degrees, the plume model (MPIC) predicts up to double the ion current densities measured experimentally. Given equation 2, we expected a doubling in the erosion as well.Improving the model fidelity, bringing it closer to the experimentally measured plume parameters would help eliminate this discrepancy and improve the agreement with the experimentally driven predictions. This could be done by expanding our experimental validation efforts to include near-field plume measurements with laser induced fluorescence. Having detailed measurements of both ion and neutral velocities at these locations would allow us to better tune the inlet conditions of the model and remove some uncertainty

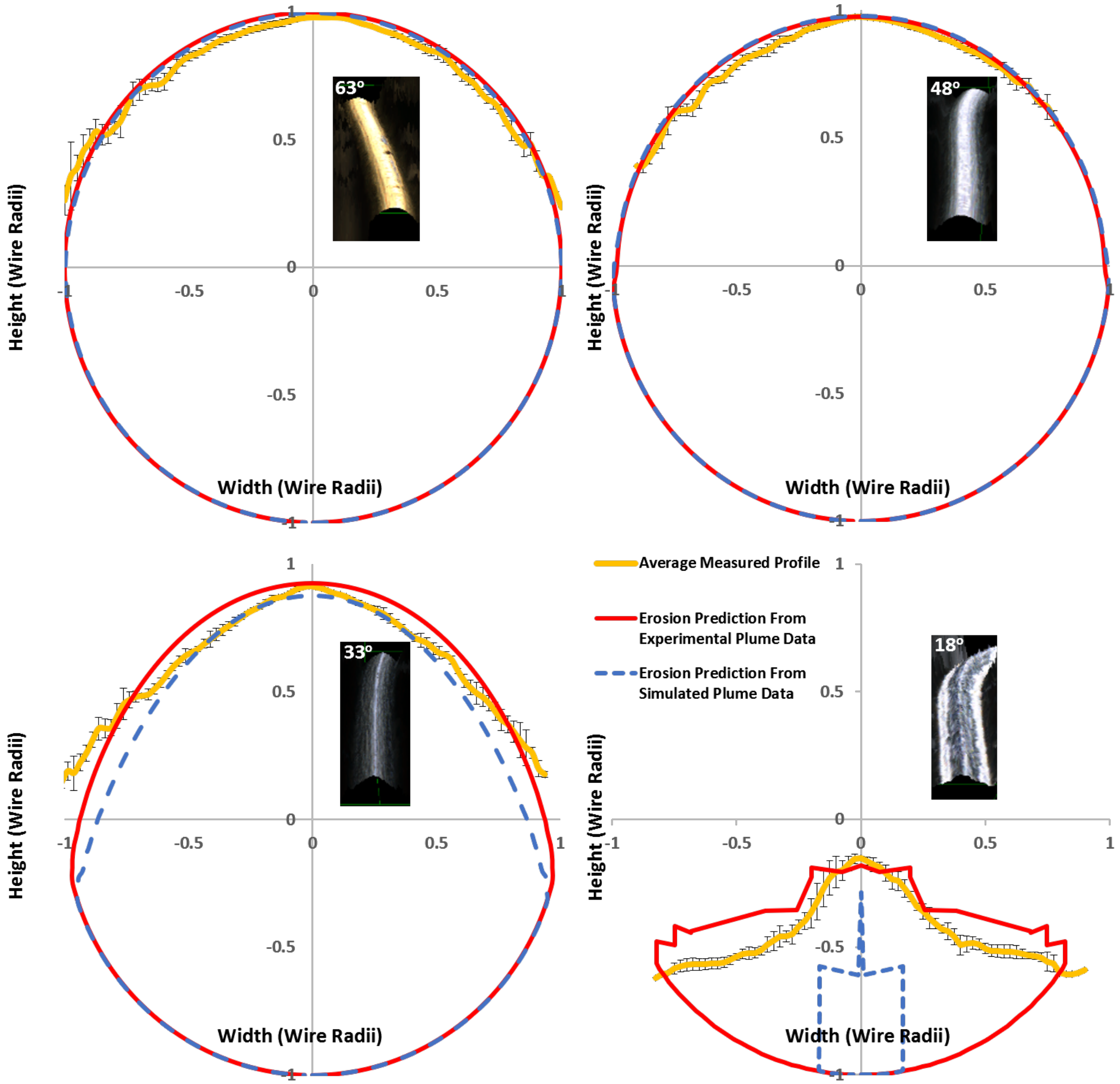

Fig. 9 Comparison between experimentally measured profiles (yellow lines) and the wire geometry predicted by the erosion model.(blue and red lines). The sputtering was calculated from the Eckstein normal incidence model [9], and the Wei [10] angular incidence models. The erosion was calculated using both the experimentally measured plasma parameters at each angular location and the calibrated plume model data.

in the inlet parameters.

As a final observation, we note that the discrepancies between the model predictions and measurements could stem from uncertainties in the models for sputtering yields. As discussed in Sec. II, there are multiple models to choose from that yield different predicted sputtering rates. These differences can drastically impact the predicted erosion (See Fig. 10). The differences in these sputtering yield models largely are the result of the different assumptions employed as well as inherent aleatoric uncertainties about the nature of the sputtering process [7]. Examples of key uncertainties relate to sample temperature and topography, sample charging, and the redepositon of sputtered material back onto sample surfaces. Given this wide range of influencing factors, it is likely that there are factors in the erosion of our samples that are not correctly captured by one or all of the models. With that said, one way to potentially control for this

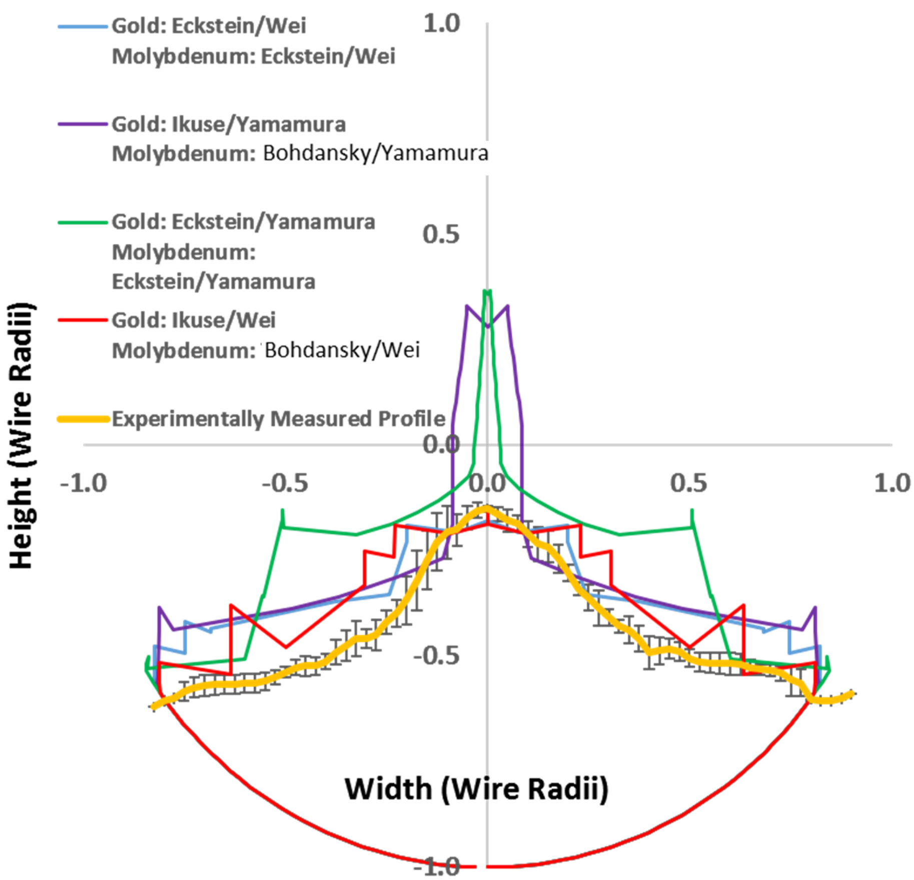

Fig. 10 The predicted wire erosion of the 18 degree sample by different combinations of sputtering models. These predictions are based on using measured plasma properties in the erosion model.

inherent uncertainty is to take an average over multiple sputtering model results. This is done in Part 1 and shown to yield exceptionally good agreement. The results are reproduced in Fig.11 to illustrate this point.

In addition to performing an average over models, there are other statistical methods for accounting for the uncertainty in sputtering yield models. For example, Yim et.al. [7] used a statistical parameter estimation technique to characterize formally with probability distributions and confidence intervals the uncertainty in the sputtering yield from the Eckstein model. This type of approach approach could be leveraged for our erosion estimates. In particular, future improvements to the model outlined in Part 1 and validated here will consist of performing rigorous forward uncertainty propagation from the sputtering yields to introduce confidence intervals to our estimates of erosion.

VI. Conclusions

The goal of this study was to provide experimental validation for the erosion model of meshed reflectors detailed in Part 1 of this report [17]. To that end, we have conducted two experiments in the plume of the H6US Hall thruster. The first experiment was a plume characterization test where we used a suite of probes to sample the downstream plume at various points in a 1m arc around the thruster. In the second experiment, we placed eight representative samples of the meshed reflector material in the plume at the same locations we characterized with the probes. The samples were exposed for a period of ten hours, after which the erosion was characterized through optical profilometry. The measured erosion profiles were then compared to the profiles predicted by the model when the measured plasma parameters were used as inputs and when simulated plasma parameters were used. We found that near the top of the wires, where the ions are striking normal to the surface, the predictions based on the experimental plume measurements remain accurate to within the profile measurement variance. Likewise, the predictions based on the plume simulation agree within the variance until the ion current densities begin to disagree with the experimental plume measurements. After this point the

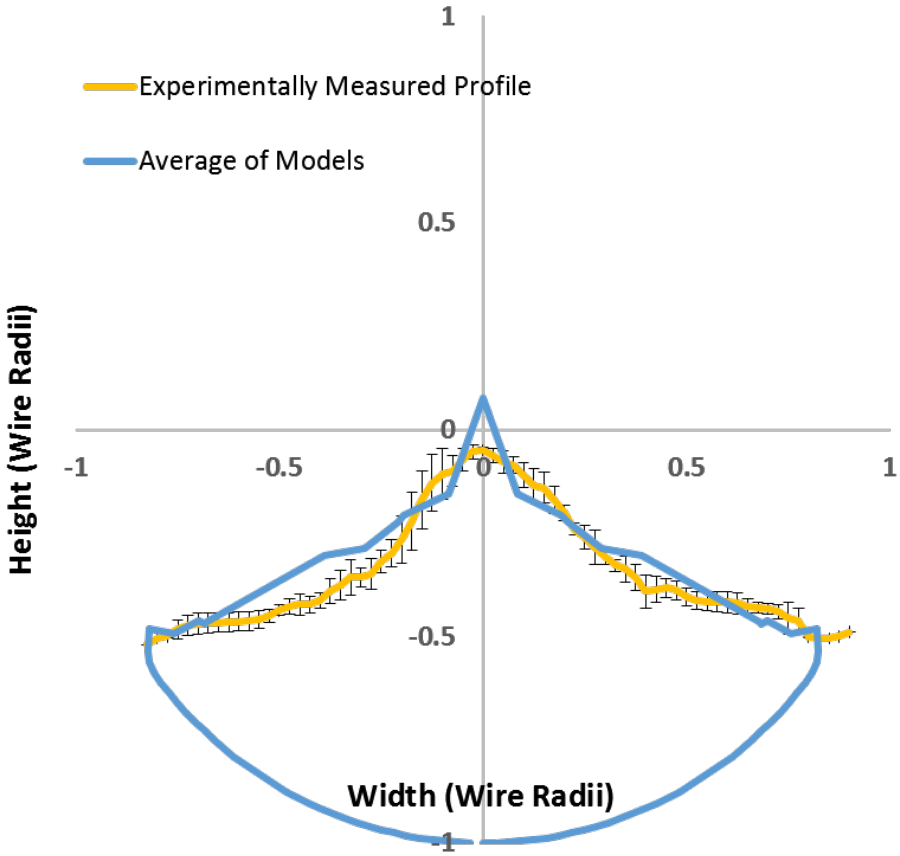

Fig. 11 The predicted wire erosion of the 18 degree sample by an average of the sputtering models. These predictions were experimentally informed.

model ceases to give physical results. At the edges of the wires, both predicted profiles agree with profile measurements when exposed to the outer wings of the plume. However, for the samples closer to thruster center line, both predictions diverged from experimental results. As the samples neared the beam, the experimental based prediction underestimated the erosion by up to 0.15 wire radii. We speculate that these discrepnacies may arise based on the impact of multiply charged ions, unaccounted for material properties, or variation in the sputtering yields models.

Despite the acknowledged minor discrepancies between model prediction and results, overall, we have found that our predictions do agree well with the actual measured erosion. This finding has direct implications for future efforts to predict spacecraft interactions for both reflectors as well as other geometries. Indeed, the erosion model developed here is not restricted to wire geometries. The method of planar discretization of target surfaces enables this model to be extensible to many other non-planar surfaces. Furthermore, the model can predict erosion as long as the plume properties near the sputtering surface are known, allowing it to be used with any type of electric propulsion system. This work thus represents a critical validation for a model that can be used to inform the design of satellites which use EP and to assess the risk of spacecraft-plume interactions.

Acknowledgments

We would like to acknowledge the funding sources which made this work possible: Rackham Merit Fellowship, Plasmadynamics and Electric Propulsion Laboratory, and the Applied Physics Program.

References

[1] Hart, William and Lev, Dan and Myers, Roger and Kolbeck, Jonathan and Keidar, Michael and Gonzalez, Jose and Choe, Wonho and Koizumi, Hiroyuki and Albertoni, Riccardo and Gabriel, Stephen and Funaki, Ikkoh. (2017). The Technological and Commercial Expansion of Electric Propulsion in the Past 24 Years.

[2] D. Y. Oh, D. E. Hastings, C. M. Marrese, J. M. Haas, and A. D. Gallimore, "Modeling of Stationary Plasma Thruster-100 Thruster Plumes and Implications for Satellite Design," Journal of Propulsion and Power, vol. 15, no. 2, pp. 345–357, 1999.

[3] Kannenberg, K., Khayms, V., Emgushov, B., Werthman, L., and Pollard, J. E., "Validation of Hall thruster plume sputter model," 37th AIAA/ASME/SAE/ASEE Joint Propulsion Conference and Exhibit, AIAA-2001-3986, 2001.

[4] Noushkam N., Basak D., Glogowski M., Crofton M. W., and Young J. A., "Sputtering effects of xenon ion thruster plume on common spacecraft materials," AIAA SPACE 2015 Conference and Exposition, AIAA-2015-4642, 2015.

[5] Boyd, I. D., and Falk, M. L., "A review of spacecraft material sputtering by Hall thruster plumes," 37th AIAA/ASME/SAE/ASEE Joint Propulsion Conference and Exhibit, AIAA-2001-3353, 2001.

[6] Fife, J. M., Gibbons, M. R., VanGilder, D. B., and Kirtley, D. E., "Initial use of a 3-D plasma simulation system for predicting surface sputtering and contamination by Hall thrusters," 33rd Plasmadynamics and Lasers Conference, AIAA-2002-2125, 2002.

[7] J. Yim, "A survey of xenon ion sputter yield data and fits relevant to electric propulsion spacecraft integration," presented at the 35th International Electric Propulsion Conference, Georgia Institute of Technology, USA, 2017, vol. IEPC-2017-060.

[8] P. Sigmund, "Sputtering by ion bombardment theoretical concepts," in Sputtering by Particle Bombardment I: Physical Sputtering of Single-Element Solids, R. Behrisch, Ed. Berlin, Heidelberg: Springer Berlin Heidelberg, 1981, pp. 9–71.

[9] Eckstein, W., and Preuss, R., "New fit formulae for the sputtering yield," Journal of Nuclear Materials, v. 320, pp. 209-213, 2003

[10] Wei, Q., Li, K.-D., Lian, J., and Wang, L., "Angular dependence of sputtering yield of amorphous and polycrystalline materials," Journal of Physics D: Applied Physics, v. 41, 172002, 2008.

[11] K. Ikuse, S. Yoshimura, K. Hine, M. Kiuchi, and S. Hamaguchi, "Sputtering yields of gold by low-energy noble gas ion bombardment," J. Phys. D: Appl. Phys., vol. 42, no. 13, p. 135203, 2009.

[12] Yamamura, Y., "An Empirical Formula for Angular Dependence of Sputtering Yields," Radiation Effects, Vol. 80, 1984, pp. 57-72.

[13] Bohdansky, J., "A universal relation for the sputtering yield of monatomic solids at normal ion incidence," Nuclear Instruments and Methods in Physics Research, B, Vol. 2, No. 1, 1984, pp. 587–591.

[14] García-Rosales, C., Eckstein, W., and Roth, J., "Revised formulae for sputtering data," Journal of Nuclear Materials, Vol. 218, No. 1, 1995, pp. 8–17.

[15] Tartz, M., Heyn, T., Bundesmann, C., Zimmermann, C., and Neumann, H., "Sputter yields of Mo, Ti, W, Al, Ag under xenon ion incidence," The European Physical Journal D, Vol. 61, No. 3, 2011, pp. 587–592.

[16] Pencil, E.J., Randolph, T., and Manzella, D.H., "End-of-Life Stationary Plasma Thruster Far-Field Plume Characterization," AIAA Paper 96-2709, July 1996

[17] Meyer, M. E., Byrne, M. P., Jorns, B. A., and Boyd, I. D. "Erosion of a meshed reflector in the plume of a Hall effect thruster, Part 1: Modeling," 55th AIAA/SAE/ASEE Joint Propulsion Conference Indianapolis, Indiana, 2019. Submitted for publication

[18] Huismann, T. D., "Improving Hall Thruster Plume Simulation through Refined Characterization of Near-field Plasma Properties," Ph.D. thesis, University of Michigan Ann Arbor, 2011.

[19] J. W. Dankanich, M. Walker, M. W. Swiatek, and J. T. Yim, "Recommended Practice for Pressure Measurement and Calculationof Effective Pumping Speed in Electric Propulsion Testing," J. Propul. Power 33, 668 (2017).

[20] Haas, J. M., Hofer, R. R., Brown, D. L., Reid, B. M., Gallimore, A. D., "Design of a 6-kW Hall Thruster for High Thrust/Power Investigation," 54th JANNAF Propulsion Meeting, Denver, CO, May 14-17, 2007

[21] Brown, D. L., Reid, B. M., Gallimore, A. D., Hofer, R. R., Haas, J. M., Larson C.W., "Performance Characterization and Design Verification of a 6-kWLaboratory Model Hall Thruster," 54th JANNAF Propulsion Meeting, Denver, CO, May 14-17, 2007

[22] Reid, B. M., Gallimore, A. D., Hofer, R. R., Li, Y., Haas, J. M., "Anode Design and Verification for a 6-kW Hall Thruster," 54th JANNAF Propulsion Meeting, Denver, CO, May 14-17, 2007

[23] M. McDonald and A. Gallimore, "High-Speed Interrogation of the Near-Field Plume of a 6-kW Laboratory Hall Thruster," 31st International Electric Propulsion Conference, Ann Arbor, MI, IEPC-2009-112, September 20-24, 2009

[24] Brown, D. L., "Investigation of Low Discharge Voltage Hall Thruster Characteristics and Evaluation of Loss Mechanisms," University of Michigan, Ph.D. Dissertation, 2009

[25] Reid, B. M., "The Influence of Neutral Flow Rate in the Operation of Hall Thrusters," University of Michigan, Ph.D. Dissertation, 2009

[26] M. McDonald, "Electron Transport in Hall Thrusters," University of Michigan, Ph.D. Dissertation, 2012

[27] Huang, W., Shastry, R., Soulas, G. C., and Kamhawi, H., “Farfield Plume Measurement and Analysis on the NASA-300M and NASA-300MS,” 33rd International Electric Propulsion Conference, IEPC-2013-057 , Electric Rocket Propulsion Society, Washington D.C., 2013